eprints@whiterose.ac.uk
https://eprints.whiterose.ac.uk/

Experimental validation of 3D magnet eddy current loss prediction in Surface Mounted Permanent Magnet Machines

Sreeju S Nair, Jiabin Wang, Tianfu Sun, Liang Chen

The University of Sheffield
S1 3JD, United Kingdom
ssnair1@sheffield.ac.uk

Robert Chin, Minos Beniakar

ABB Corporate Research
SE-721 78 Västerås, Sweden
robert.chin@se.abb.com

Abstract— **This paper presents the experimental validation of 3D Fourier method employed for predicting magnet eddy current loss in surface mounted permanent magnet (SPM) machines. The magnet loss is measured for a 12-slot,14-pole SPM machine from experimental tests when the machine is operated with inverter under locked rotor conditions by repeating tests with two rotors, one with magnets and one without. The eddy current loss associated with each significant harmonic in the captured armature currents is predicted separately employing the developed method and the total magnet loss is evaluated by applying the principle of superposition. The magnet loss at real operating conditions of the machine is predicted from the method using the phase current captured when the SPM is operating at its maximum speed conditions. The result is used as example to devise an effective means of further reduction in the total magnet loss.**

Index Terms—**Eddy currents, finite element method, imaging method, permanent magnet, subdomain model.**

I. Introduction

The rotor magnets of permanent magnet (PM) machines used in high speed and high power density applications are exposed to increased rate of alternating magnetic field and incur eddy current loss. Eddy currents are more pronounced in magnets especially at high speeds for SPM machines with modular winding configurations [1, 2], fed by 3-phase inverter drives with pulse width modulations (PWM). An accurate prediction of magnet losses at the design stage, not only gives better efficiency evaluation, but also may prevent its excessive temperature rise and hence reduce the risk of partial demagnetization[3].

There are a number of analytical and computationally efficient quasi numerical methods discussed in literature [4-7] to predict magnet eddy current loss at worst operating conditions of SPM machines. The state-of-the art finite element (FE) based commercial tools for 2D and 3D analysis of electromagnetic fields have reached a high level of maturity and hence the accuracy of analysis is guaranteed as long as the machine model is correctly formulated. Hence, almost all publications in literature on prediction of eddy current losses in rotor magnets employ 3D FE analysis as a means of validating the developed computationally efficient methods. From scientific point of view, rotor eddy current loss validation based on numerical analysis is far from the ideal. The challenges for the experimental validation, however, arise from the fact that the amount of rotor eddy current loss is relatively small in a well-designed PM machine and it cannot be separated from other loss components such as the iron loss and mechanical loss by direct measurements.

Attempts for indirect measurement of eddy current loss density in rotor magnets have been reported in literature. Since the loss density contributes to the increases in temperature, indirect magnet loss density measurement by thermometric method is described in[8] based on the rate of temperature rise measured by temperature sensors through low noise slip-rings. A similar method is carried out for rotor loss measurements in [9, 10] for validating analytical and FE based loss predictions. However, the accuracy of these techniques is quite limited since the change in the contact resistance of the slip rings and brushes introduces significant noise. This problem may be avoided by carrying out the temperature measurements each time when the machine stops its operation as reported in [11]. However, inevitable delay between a given operating condition and the measurement is introduced and the accuracy is also compromised. The thermometric method can only estimate the loss density based on the thermal property and geometry of the magnets, and its accuracy is often affected by intrusive nature of the sensor deployment and no-uniform temperature distribution in the magnets as well as the heat exchanges with other regions[12].

There are also a few publications [12-15] in the literature which measures eddy current loss of magnets placed inside a solenoid coil with sinusoidal excitation. Since the magnets are stationary, the thermal measurements are carried out at different currents and frequencies without need for brushes and slip rings. These experiments are used to investigate the reduction in magnet loss with increase in segmentations. In [16] the total iron loss and eddy current loss in rotor magnets are separated from the other machine losses while proposing techniques for reducing rotor eddy current loss in an interior permanent magnet (IPM) machine with concentrated windings. However, it is not possible to separate the rotor eddy current loss from the measurements. In [17] eddy current loss in rotor magnets are estimated by subtracting FE predicted stator iron loss from the measured sum of total iron loss and eddy current loss. The rotor eddy current loss in an SPM machine due to inverter PWM operations is separated in [18] by subtracting the loss of the machine with the magnets from that without the magnets and employing appropriate control of armature currents and voltages at locked rotor

conditions.

Computationally efficient techniques for predicting 3D eddy current loss in rotor magnets of SPM machines at low and high frequencies have been proposed [19-21]. The method establishes the distribution of eddy current sources in the form of 3D Fourier series in x, y, z directions, and evaluates eddy current loss components based on Fourier expansion in three dimensions. The 3D eddy current source distribution accounting eddy current reaction effect is included in [22] to predict the eddy current loss at high frequencies. However, these methods are validated only by 3D FE analysis. In addition, the effect of high frequency switching harmonics on causing magnet loss is not quantified by experiments in general.

In this paper the techniques for predicting 3D eddy current loss in rotor magnets of permanent magnet machines are validated by experiments. The magnet eddy current loss is separated from other losses by employing locked rotor tests with and without magnets on a 14-pole, 12 –slot PM machine. In addition, the magnet loss accounting all the armature harmonics at the real operating conditions is evaluated by employing phase currents measured from the experiments at the maximum speed conditions in the proposed method. It is shown that the contribution of the switching harmonics in the phase currents to the total eddy current loss can become significant and reaches 50% at the maximum speed conditions.

II. PREDICTION OF 3D EDDY CURRENT LOSS IN ROTOR MAGNET

The computationally efficient technique for predicting 3D eddy current loss in rotor magnets of an SPM machine is outlined for reader's convenience. It is assumed that the magnetic field in rotor magnets is two dimensional with its radial and tangential components denoted by B_r and B_t, respectively. The eddy current in the rotor magnets is induced by time derivatives of the magnetic field, and they are denoted by S ($S_x = \partial B_t / \partial t$, $S_y = \partial B_r / \partial t$) as the sources of the induced eddy current. It has been shown in [19] and [20] that by satisfying the boundary conditions of the eddy current flow on the magnet surfaces, the source distribution within the magnets can be expressed as 3D Fourier series of the following form:

$$S_x = \sum_{m=1}^{\infty}\sum_{n=1}^{\infty}\sum_{k=1}^{\infty} a_{(m,n,k)} cos\left(m\frac{\pi}{L_x}x\right) sin\left(n\frac{\pi}{L_y}y\right) sin\left(k\frac{\pi}{L_z}z\right) \tag{1}$$

$$S_y = \sum_{m=1}^{\infty}\sum_{n=1}^{\infty}\sum_{k=1}^{\infty} b_{(m,n,k)} sin\left(m\frac{\pi}{L_x}x\right) cos\left(n\frac{\pi}{L_y}y\right) sin\left(k\frac{\pi}{L_z}z\right) \tag{2}$$

where L_x, L_y and L_z are the magnet dimensions in the tangential (x), radial (y) and axial (z) directions, respectively. m, n, k are the harmonic orders in the x, y, z directions, respectively. $a(m,n,k)$ and $b(m,n,k)$ are Fourier coefficients which can be calculated by the expressions given in [20]. (1)

and (2) allows to compute the source harmonic components within the magnets by applying FFT in the magnet volume.

By introducing a current vector potential A defined as $A = \nabla \times J$, where J is the eddy current density, its solutions $A = (A_x, A_y)$, which satisfy Poisson's equation,

$$\nabla^2 A = -\sigma S \tag{3}$$

under the Coulomb gauge $\nabla \cdot A = 0$ are given by,

$$A_x = \sum_{m=1}^{\infty}\sum_{n=1}^{\infty}\sum_{k=1}^{\infty} c_{(m,n,k)} cos\left(m\frac{\pi}{L_x}x\right) sin\left(n\frac{\pi}{L_y}y\right) sin\left(k\frac{\pi}{L_z}z\right) \tag{4}$$

$$A_y = \sum_{m=1}^{\infty}\sum_{n=1}^{\infty}\sum_{k=1}^{\infty} d_{(m,n,k)} sin\left(m\frac{\pi}{L_x}x\right) cos\left(n\frac{\pi}{L_y}y\right) sin\left(k\frac{\pi}{L_z}z\right) \tag{5}$$

where $c(m,n,k)$ and $d(m,n,k)$ are the coefficients associated with (n, m, k)[th] harmonic given in [20] .
Consequently, the eddy current density $J = (J_x, J_y, J_z)$ can be derived from

$$\nabla \times A = J \tag{6}$$

as,

$$J_x = \sum_{m=1}^{\infty}\sum_{n=1}^{\infty}\sum_{k=1}^{\infty} e_{(m,n,k)} sin\left(m\frac{\pi}{L_x}x\right) cos\left(n\frac{\pi}{L_y}y\right) cos\left(k\frac{\pi}{L_z}z\right) \tag{7}$$

$$J_y = \sum_{m=1}^{\infty}\sum_{n=1}^{\infty}\sum_{k=1}^{\infty} h_{(m,n,k)} cos\left(m\frac{\pi}{L_x}x\right) sin\left(n\frac{\pi}{L_y}y\right) cos\left(k\frac{\pi}{L_z}z\right) \tag{8}$$

$$J_z = \sum_{m=1}^{\infty}\sum_{n=1}^{\infty}\sum_{k=1}^{\infty} q_{(m,n,k)} cos\left(m\frac{\pi}{L_x}x\right) cos\left(n\frac{\pi}{L_y}y\right) sin\left(k\frac{\pi}{L_z}z\right) \tag{9}$$

where, $e_{(m,n,k)}, h_{(m,n,k)}$ and $q_{(m,n,k)}$ are the coefficients associated with (n, m, k)[th] harmonic for the eddy current densities which are derived from $a_{(m,n,k)}$ and $b_{(m,n,k)}$ after the operations defined in (3) and (6).

Once the eddy current distribution is known the total eddy current loss at a given time instant is the sum of the losses associated with each harmonic component:

$$P_{eddy} = \sum_{m=1}^{\infty}\sum_{n=1}^{\infty}\sum_{k=1}^{\infty} \frac{1}{8} \int_0^{2L_x}\int_0^{2L_y}\int_0^{2L_z} \left(\begin{array}{c} J_{x(m,n,k)}^{2} \\ +J_{y(m,n,k)}^{2} \\ +J_{z(m,n,k)}^{2} \end{array} \right) dxdydz \tag{10}$$

$$= \sum_{m=1}^{\infty}\sum_{n=1}^{\infty}\sum_{k=1}^{\infty} \left\{ p_{1(m,n,k)} + p_{2(m,n,k)} + p_{3(m,n,k)} + p_{4(m,n,k)} + p_{5(m,n,k)} \right\}$$

The coefficients, $c_{(m,n,k)}$, $d_{(m,n,k)}$, $e_{(m,n,k)}$, $h_{(m,n,k)}$, $q_{(m,n,k)}$ for the current vector potential and eddy current densities, and $p_{1(m,n,k)}$ - $p_{5(m,n,k)}$ for the total eddy current loss are all arithmetic functions of the harmonic order and magnet dimensions which are given in [20]. The method of prediction of high frequency eddy current loss associated with high frequency harmonics is detailed in [22]. With this technique, the prediction of 3D

eddy current loss in the rotor magnets can be performed in a few minutes in contrast to a few days with 3D time-stepped transient FE analysis.

III. EXPERIMENTAL TESTING TO MEASURE THE MAGNET LOSS

A. Machine Specifications and Rotor Prototyping

The 3D magnet loss prediction technique developed is experimentally validated on a 10kW (peak), 14-pole,12-slot SPM machine designed for EV traction applications [23]. The cross-section of the machine illustrating its winding configuration is shown in Fig.1. The design specifications of the SPM are given in Table.1, and the performance indicators of the 14-pole,12-slot SPM is detailed in [23].
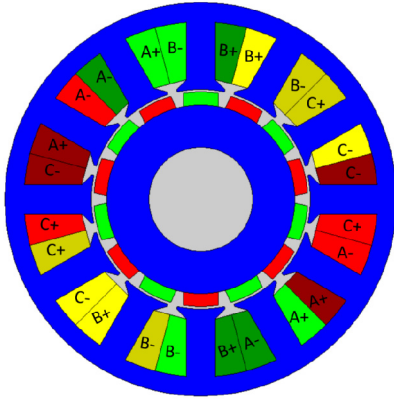

Fig.1.Cross-section of the 14-pole, 12-slot SPM machine.

Table I
Design Specifications of the 10kW, 14-pole, 12-slot SPM

Design parameter	Unit	Value
Stator outer radius	mm	75.58
Motor stack length	mm	122.0
Air-gap length	mm	1.0
Rotor radius	mm	41.19
Length of magnet	mm	14.0
Width of magnet	mm	5.8
No. of turns per coil	-	8
No. of coils per phase	-	4
Magnet (NdFeB-N35SH) -Br	T	1.22
No of magnet segments (axial)	-	3

To circumvent the difficulty of loss separation, the tests are to be carried out under locked rotor conditions. Two rotors are built, one with magnets and the other without magnets, as shown in Fig.2 (a) and (b), respectively. The adhesive applied in between the magnets and the rotor core will provide a thin layer of electrical insulation between the two. The magnets were pasted non-magnetized. Therefore, when the motor windings are excited with appropriate current under locked rotor conditions, the magnetic field distributions in the machine with two different rotors are essentially almost the same, and the only difference is due to induced eddy current in the magnets on one of the rotor

B. Test Procedure and Loss Measurements

Initially the testing was carried at the locked rotor condition with the rotor without magnets. The machine

windings were supplied by an inverter with 45A (peak) phase currents at 400Hz. Space vector modulation at 8kHz switching frequency is implemented for the inverter while generating the 3-phase currents under current feedback control. This frequency is selected because in real operation of the machine at 3429 rpm, the backward rotating harmonic which is the main cause of the eddy current loss in the rotor has a similar frequency seen by the rotor.

Measurements were taken at three different angular positions of the rotor each separated by 60^0 (mech.). Theoretically, the measured loss will be independent of the locked rotor position if the machine windings are perfectly symmetrical and the air gap is uniform. In reality, these conditions may not be true due to manufacturing tolerance, and hence the measurements at three positions will yield a more accurate and consistent average.
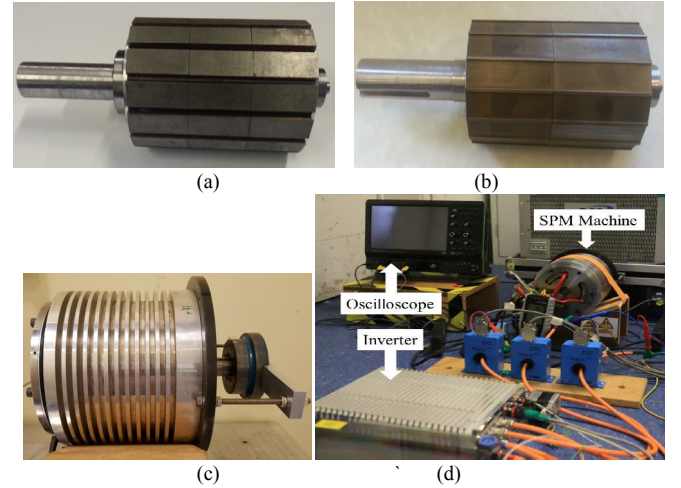

Fig 2. Prototype rotors and experimental setup. (a) without magnet. (b) with magnet. (c) machine assembly with locked rotor. (d) Experimental setup.

The experiment was repeated employing the rotor assembled with permanent magnets for the same phase current and the measurements were taken at the same three different rotor positions and also at the same winding temperatures as measured in the previous case without magnets. Winding temperature was maintained the same before taking each measurement to make sure the winding copper loss is almost the same throughout the test. For both the tests power input to the machine was measured from the power analyzer configured in 2 Wattmeter method and the phase current waveforms were captured using the high resolution, high bandwidth oscilloscope. The test was repeated when the machine windings were supplied with 50A peak phase currents at 400Hz and also with 45A peak phase currents at 450Hz. The 3 test conditions were chosen as the magnet loss expected is sufficient large for experimental measurements with good accuracy as confirmed from the 2D FE simulations. The fully assembled machine with rotor locked and the whole experimental set is illustrated in Fig.2

The phase current magnitudes in the three tests are chosen such that the magnet losses incurred at these conditions are sufficiently large for experimental measurements. It is also

ensured that these three tests will not result in an excessive temperature rise within the machine at the locked rotor conditions. In addition, the winding temperature rise is kept low as possible, thus avoiding large variations in the copper loss because of change in electrical resistivity.

The measured power inputs to the machine under locked rotor conditions with and without magnets for the three test cases are listed in Table. II. The resultant power losses are the average of the power losses measured at the three different angular positions. The phase currents captured from the experiments for the three test cases are shown in Fig.3.

TABLE II
Power Input Measured from the Experimental Tests
(case.1=400Hz,45A, case 2= 400Hz,50A, case3= 450Hz,50A)

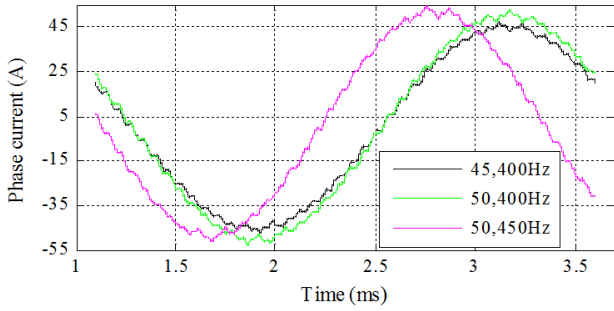| Case	Temperature (deg. C)	Average Power loss without magnets-W1 (W)	Average Power loss with magnets-W2 (W)
1	30	147.14	167.27
2	37	175.27	199.70
3	40	197.47	228.87

Fig.3.Phase current captured during the experiments for the three test cases with magnets.

It is observed that there is a small difference in the phase currents measured from the two experiments with and without magnets for all the three test cases due to current control error of the inverter. The variations in the phase currents captured from the two experiments for the case-2 are shown in Fig.4. Hence a correction towards the copper loss is calculated based on the fundamental of each phase currents. This is included in the measured power loss for the experiments with magnets. The evaluation of the power losses to the machine illustrating this correction is shown in Table. III.

For each test without the magnets, the measured power loss should be the sum of the iron loss in the stator and rotor cores, and the winding copper loss. For each test with magnets, the measured power loss should be the sum of the iron loss in the stator and rotor cores, the winding copper loss and magnet eddy current loss. Since the two tests without and with magnets are performed under the same excitation current and frequency, the iron loss and copper loss should be almost the same. Therefore, magnet eddy current loss is evaluated from the difference in the power losses measured from the two tests, with and without magnets after incorporating correction in the copper loss previously described. That is,

Eddy current loss in magnets = W2-W1

where W1 denotes the measured power loss without magnets, and W2 denotes the measured power loss with magnets after correcting the small difference in copper loss. Hence the magnet loss measured from the 3 test cases are found be equal to 19.09, 22.77and 29.61W respectively.

TABLE III
CORRECTION IN COPPER LOSS FOR THE MINOR VARIATION IN THE PHASE CURRENTS

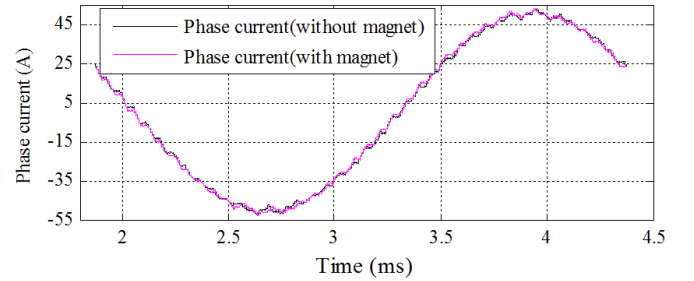| Case	Change in fundamental current with magnets (A)	Correction of copper loss (W)	Power loss with magnets, corrected-W2. (W)
1	0.29	1.027	166.24
2	0.38	1.67	198.03
3	0.45	1.81	227.17

Fig.4. Comparison of phase currents captured from the two experiments for the case.2 (50A,400Hz).

IV. MAGNET LOSS PREDICTION AND COMPARISON OF RESULTS

The Magnet losses are also predicted for the SPM machine at the 3 test cases by the method briefly described in section II employing the phase currents captured from the experiments. FFT is performed for the one complete cycle to evaluate the harmonic contents present in the measured phase currents for all the three different test conditions. Fig.5. shows the phase current spectrum for the three test cases with magnets. It is observed that the total harmonic distortions (THD) are 3.1, 3.1 and 3.4% for the case 1, 2 and 3, respectively.

3-D loss predictions are performed using the technique described in [20] and [22]. For the machine under consideration, each magnet attached to the mesh grids discretized into sixty-four divisions along the x- and thirty-two divisions along y-directions. Magnet loss at fundamental frequency is evaluated for the axial segments from 1 to 10 and the results are shown in Fig.6. The points marked in black indicate the magnet losses predicted for the prototype machine under tests with 3 axial segments.

It is observed that for all the harmonic contents of frequency above 7200Hz, the eddy current sources are found to have significant variations along the axial plane due to eddy current reaction effect. Hence for evaluating the loss associated with these components axial variations of S_y is incorporated before implementing in the 3D Fourier method

as described in [22]. The predicted variations of magnet loss with increase in axial segmentations for the major high frequency harmonics evaluated are shown in Fig.7. Again, the points marked in black indicate the losses predicted for the test machine with 3 axial segments.

(a)   Case.1
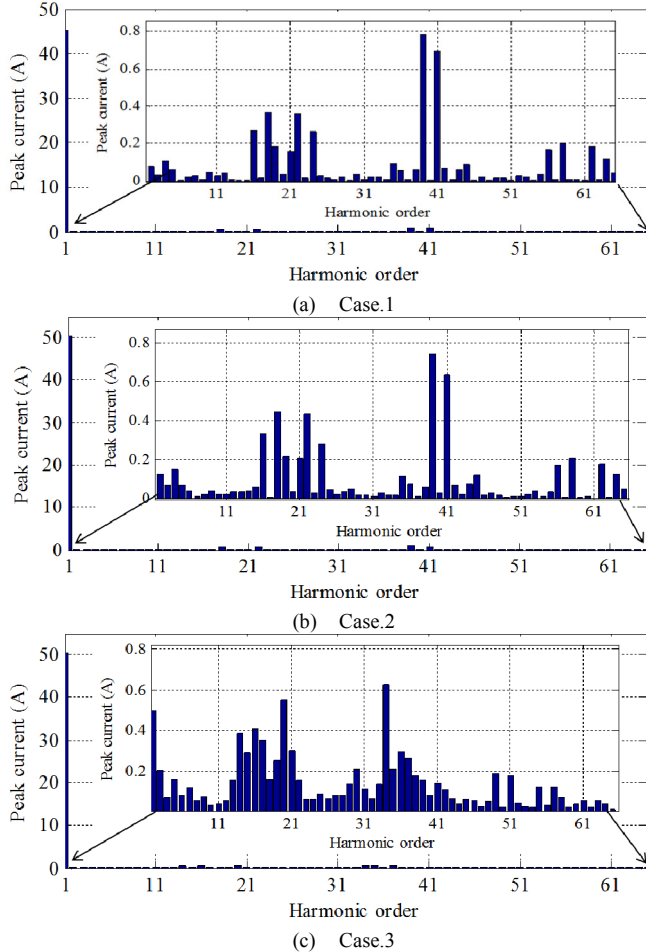

(b)   Case.2

(c)   Case.3

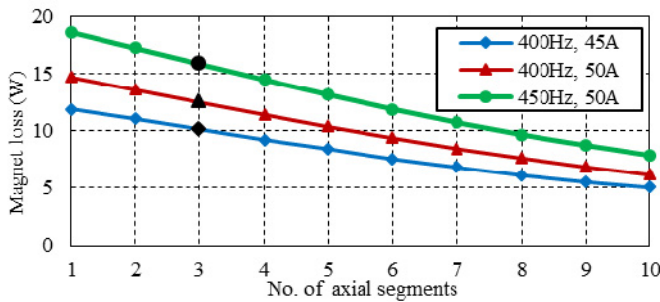Fig.5 Harmonic spectrum of the phase currents captured from the three test cases.

Fig.6. Variation of magnet losses due to fundamental with increase in axial segmentations evaluated from the 3D Fourier method for the three test cases.

It is worth noting that the increase in the magnet losses due to high frequency current harmonics with initial increase in the number of axial segments [21] is not observed here. This is because the low circumferential width (L_x=14mm) of the magnet reduces the eddy current reaction effect and hence the difference in the time derivations of flux density along the

middle and the axial edges is relatively small. For example, Fig.8 compares the flux density derivative variations along the middle of the magnet and its axial ends when the magnet pole arc angle (Bm) is increased from 132^0 (used in the tests) to 175^0. The resultant variations of the magnet loss with increase in axial number of segments for these cases are shown in Fig.9.

(a) 400Hz,45A.

(b) 400Hz,50A.

(c) 450Hz,50A.
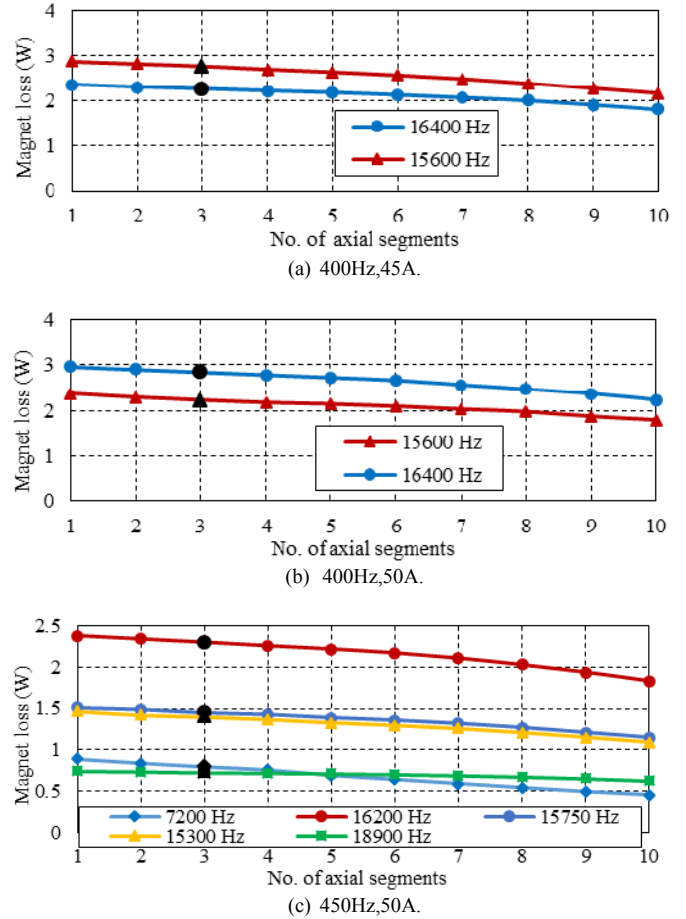
Fig.7. Predicted loss variations due to high frequency current harmonics with increase in axial number of segments.

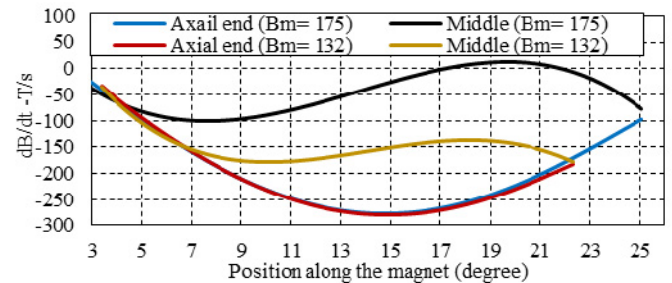Fig.8.Comparison of time derivatives of flux density along the axial end and the middle of the magnet with two pole arc angles when supplied with 0.65A at 16200Hz.

When the pole arc angle is 175^0, the high frequency eddy current loss increases slightly with initial increase in the number of axial segments. This is because strong eddy current reaction tends to reduce magnet loss but the initial axial

segmentation weakens the eddy current reaction, and hence increases the loss. With further increase in axial segmentation, the resistance to eddy current flow is significantly increased, and hence the eddy current loss decreases monotonically.

As the saturation effect is not significant at the given operating conditions, the total magnet loss under the locked rotor condition can evaluated from the summation of individual harmonic losses. The magnet losses measured from the experiments and predicted by the proposed method for the three test cases are compared in Table IV.
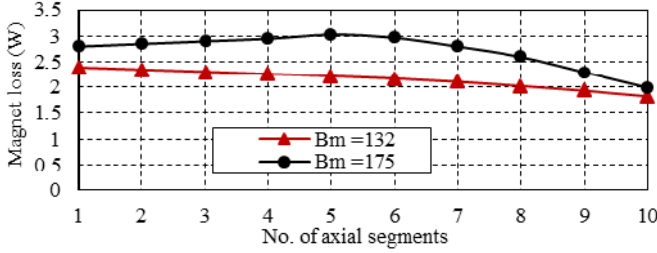

Fig.9. Comparison of magnet loss with increase in axial segmentation for pole arc angles 132^0 and 175^0 when supplied with 0.65A at 16200Hz.

TABLE IV
COMPARISON OF MAGNET LOSS MEASURED FROM EXPERIMENTS AND PREDICTED BY 3D FOURIER METHOD

Test case	Magnet loss measured (W)	Magnet loss predicted (W)	Error(%)
Case.1	19.09	17.52	8.22
Case.2	22.76	21.45	5.76
Case.3	29.61	27.45	7.28

It is observed that the experimental results agree closely with the results obtained from the prediction. The difference in measured and predicted losses may be attributed to a number of factors. First, the end winding effect is neglected in the proposed prediction method. Minor changes in iron losses in two tests with and without magnets may also exist. In addition, the conductivity of magnets used in the prediction based on datasheet may be different from that of the real magnets. From the predictions, the total magnet loss can be separated into the component associated with the fundamental and those due to switching harmonics as given in Table V.

TABLE V
PREDICTED MAGNET LOSS ASSOCIATED WITH FUNDAMENTAL AND SWITCHING HARMONICS

Test case	Fundamental (W)	Switching harmonics (W)
Case.1	10.17	7.35
Case.2	12.55	8.90
Case.3	15.89	11.57

It is worth nothing from Table V that the contribution of switching harmonics towards the magnet eddy current loss is significant and is over 40% of the total magnet loss for all the three test cases even though the THD is just over 3%.

V. MAGNET LOSS AT THE MAXIMUM SPEED CONDITIONS OF THE MACHINE.

As the 3D Fourier method has been validated by experiments at the locked rotor conditions, it can be employed to predict the magnet loss at any operating conditions of the SPM machine. Experiments are conducted to validate the performance characteristics of the 14-pole, 12-slot SPM machine [23]. Phase currents are captured and the corresponding torque is measured at various operating conditions of the machine. Likewise, in the magnet loss validation experiments discussed previously, 8kHz switching frequency is employed for the inverter for the performance validation experiments.

The actual magnet losses in the fractional slot SPM machine could be significantly due to the interaction of forward and backward rotating harmonics in the armature reaction [24] as well as the high frequency switching harmonics. Hence, the magnet loss is predicted by employing the phase currents captured when the machine is delivering 7 kW power (15 Nm) at 4500 rpm. This particular operating point is chosen as it corresponds to the maximum speed of operation under field weakening [23]. The magnet loss is expected to be much larger at this operating condition because of the high fundamental frequency and high THD. The phase current recorded at the above operating conditions of the machine for one full cycle is shown in Fig.10. At this operating condition the phase current demand to the inverter control was 74.5A (I_q =35A, I_d =-65.75A).

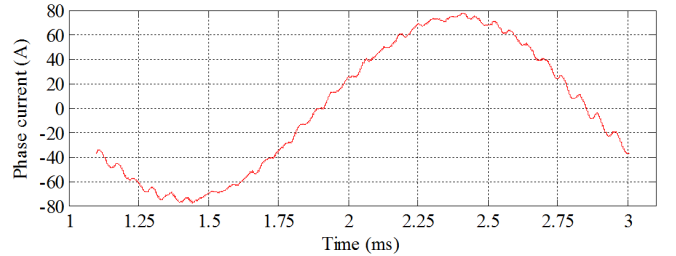Fig.10. Phase current captured for a cycle when the 14-pole,12-slot SPM machine is operating at maximum speed (4500 rpm) and delivering 7kW power.
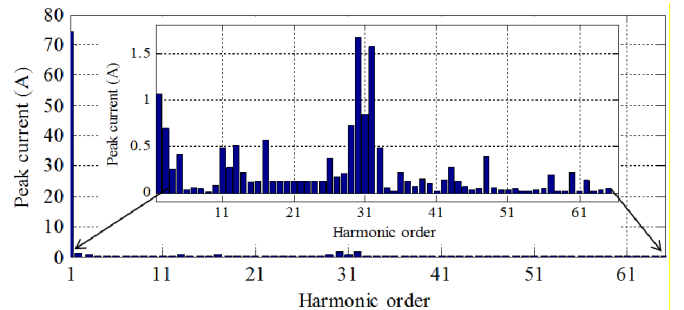

Fig.11. Harmonic spectrum of the phase current captured at the maximum speed.

FFT is performed to evaluate the different harmonic contents in the phase currents obtained at this real operating condition. THD for the phase current is observed as 4.5%.

Fig.11 shows the phase current spectrum for the phase current at the maximum speed conditions.

The magnet loss is predicted for each major harmonic frequency content available in the phase current captured. As discussed previously, the 3D magnet loss is evaluated employing the axial source variations for all high order harmonics which are affected by eddy current reaction effect. The predicted magnet losses associated with all the significant harmonics under the operating condition is consolidated in Table VI. It should be noted that that the presence of the even order time harmonics in the phase current is due to imperfect symmetry of the 3-phase winding and in inverter. As the core saturation associated with phase current is not significant in the SPM machine for the operating condition considered, the superposition is employed to evaluate the total magnet eddy current loss.

It can be seen that the magnet loss associated is 105.87 W at the maximum speed operation. Also the table above shows that the loss associated with higher order harmonics is close to 41.37% of the total loss at the operating conditions specified. Hence it is clear that the loss associated with the switching harmonics is significant and cannot be neglected while predicting the total magnet loss at the real operating conditions of the machine. For example, the amplitude of the 16800Hz harmonic is about 2.12% of the fundamental but it incurs 25.59% of the loss associated with the fundamental.

TABLE VI
MAGNET LOSS FOR THE MAJOR HARMONIC CONTENTS FOR OPERATION AT MAXIMUM. SPEED.

Fundamental and other harmonics order	Frequency (Hz)	Peak Current (A)	3D Loss (W)
1	525	74.29	61.69
2	1050	1.07	0.18
3	1575	0.69	0.15
5	2625	0.42	0.16
11	5775	0.48	0.45
13	6825	0.51	0.62
17	8925	0.57	0.67
26	13650	0.37	0.32
29	15225	0.72	1.57
30	15750	1.67	15.27
31	16275	0.87	3.57
32	16800	1.57	15.79
33	17325	0.49	0.97
43	22575	0.27	1.17
48	25200	0.39	1.37
57	29925	0.19	0.85
60	31500	0.25	1.07
Total	-	-	105.87

A 3D model of the 14-pole, 12-slot SPM machine is constructed in CEDRAT- FLUX 3D as described in [23]. 3D transient FE analysis is carried out by employing the phase current given Fig.10 over 60^0 electric angular divisions along $1/6^{th}$ of an electrical cycle and the results are averaged to predict the 3D eddy current loss within the magnets. It is observed the total magnet loss predicted by 3D FEA at this condition is 101.57W.

The similarity of the results obtained justifies the method of superposition applied to the loss associated with individual harmonics while predicting the total magnet loss. The miss match in the results can be attributed to the saturation of the core material as a result of increased phase currents in the SPM machine. The difference in results can also be the attributed to the lower number of angular discretization in 3D FEA for each cycle of higher order harmonics to avoid enormous increase in the computation time.

VI. CIRCUMFERENTIAL SEGMENTATION FOR FURTHER REDUCTION IN MAGNET LOSS

The increased magnet loss at the real operating conditions suggests the designer to further segment the magnets and thus reduce the total eddy current loss. While the contribution of higher order harmonics is significant, as seen from Fig.7 that a small increase in the number of axial segments (from the existing 3) will result only in a little reduction in the loss, axial segmentation is not preferred for further reduction of magnet loss. This is because a minor increase in axial segmentation cannot result in a large increase in the resistance towards the eddy current flow.
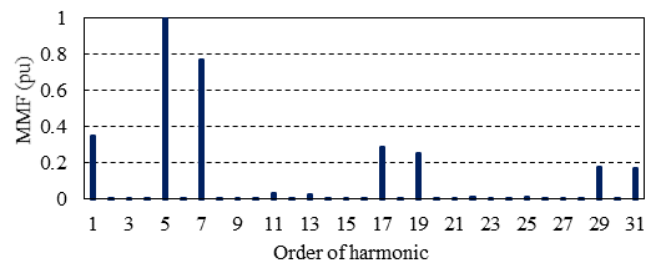

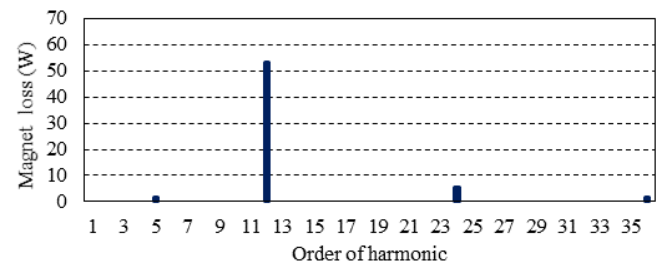Fig.12. Normalized MMF space harmonic distribution for the 14-pole,12-slot SPM machine.

Fig.13. Magnet loss associated with time harmonic seen in the rotor due to fundamental MMF space harmonics in the 14-pole,12-slot SPM machine at maximum speed

In the 14-pole, 12-slot fractional slot machine under study, the MMF space harmonics due to fundamental current are of the order 1, 5, 7, 11, 13, 17, 19, 23, 29, 31… etc. as shown in Fig. 12. It can be shown that these space harmonics give rise to the dominant time harmonics seen by the rotor of the order 6, 12, 24, 36… . The loss associated with different space harmonics when supplied only with the fundamental phase current at the maximum speed conditions is shown in Fig.13. It can be seen that the 12th order is dominant and its wavelength is 20.04mm. When the magnet per pole is not segmented circumferentially, the wavelength of the dominant frequency harmonic is close to the unsegmented width of 14.0mm. This will result in large eddy current loss. Therefore,

a larger reduction in the magnet loss [20, 25] can be achieved by circumferential segmentation.. The circumferential segmentation also breaks periodic return paths of the eddy current flow due to high frequency time harmonics in the phase current, and hence reduces their losses.

Hence, for example, an increase in the magnet segments to four along the circumferential direction and keeping the same 3 axial segments as before has resulted in the reduction of total magnet loss to 20.59W at the maximum speed condition of the PM machine. Also it is observed that the magnet loss associated with the fundamental and higher order harmonics are 10.17W and 10.42W, respectively. As discussed previously, the result proves the method of circumferential segmentation has significantly reduced the total magnet loss associated with both the fundamental and higher order harmonics.

VII. CONCLUSION

The computationally efficient 3D Fourier method for predicting eddy current loss in rotor magnets has been experimentally validated on the 14-pole, 12-slot SPM machine by employing locked rotor tests. Due to PWM operation of inverter fed drives, the switching harmonics in phase currents are accounted in the prediction. It is observed that the contribution of the switching harmonics in the phase currents to rotor eddy current loss can become significant even though phase current THD is relatively small. The eddy current loss due to switching harmonics can be close to 50% of the total eddy current loss at the maximum speed of operation. The accuracy of the results proves the superposition method can be employed to predict the total magnet loss associated with all the phase current time harmonics in SPM machines. By analyzing the wavelength of the dominant time harmonics seen in the rotor, the method of circumferential segmentation can be devised to effectively reduce the total magnet loss by breaking the periodic eddy current return paths.

REFERENCES

[1] K. Atallah, J. Wang, and D. Howe, "Torque-ripple minimization in modular permanent-magnet brushless machines," *IEEE Trans. Ind. Appl.,* vol. 39, pp. 1689-1695, 2003.

[2] R. Wrobel and P. H. Mellor, "Design Considerations of a Direct Drive Brushless Machine With Concentrated Windings," *IEEE Trans. Energy Convers.,* vol. 23, pp. 1-8, 2008.

[3] P. Zhou, D. Lin, Y. Xiao, N. Lambert, and M. A. Rahman, "Temperature-Dependent Demagnetization Model of Permanent Magnets for Finite Element Analysis," *IEEE Trans. Magn.,* vol. 48, pp. 1031-1034, 2012.

[4] N. Bianchi, S. Bolognani, and E. Fornasiero, "An Overview of Rotor Losses Determination in Three-Phase Fractional-Slot PM Machines," *IEEE Trans. Ind. Appl.,* vol. 46, pp. 2338-2345, 2010.

[5] M. Mirzaei, A. Binder, B. Funieru, and M. Susic, "Analytical Calculations of Induced Eddy Currents Losses in the Magnets of Surface Mounted PM Machines With Consideration of Circumferential and Axial Segmentation Effects," *IEEE Trans. Magn.,* vol. 48, pp. 4831-4841, 2012.

[6] J. D. Ede, K. Atallah, G. W. Jewell, J. Wang, and D. Howe, "Effect of Axial Segmentation of Permanent Magnets on Rotor Loss in Modular Permanent-Magnet Brushless Machines," *IEEE Trans. Ind. Appl.,* vol. 43, pp. 1207-1213, 2007.

[7] K. Yamazaki and Y. Fukushima, "Effect of Eddy-Current Loss Reduction by Magnet Segmentation in Synchronous Motors With Concentrated Windings," *IEEE Trans. Ind. Appl.,* vol. 47, pp. 779-788, 2011.

[8] Z. Q. Zhu, K. Ng, N. Schofield, and D. Howe, "Improved analytical modelling of rotor eddy current loss in brushless machines equipped with surface-mounted permanent magnets," *IEE Electr. Power Appl.,* vol. 151, pp. 641-650, 2004.

[9] D. A. Wills and M. J. Kamper, "Analytical prediction of rotor eddy current loss due to stator slotting in PM machines," in *2010 IEEE Energy Conversion Congress and Exposition*, 2010, pp. 992-995.

[10] K. Yamazaki, Y. Kato, T. Ikemi, and S. Ohki, "Reduction of Rotor Losses in Multilayer Interior Permanent-Magnet Synchronous Motors by Introducing Novel Topology of Rotor Flux Barriers," *IEEE Trans. Ind. Appl.,* vol. 50, pp. 3185-3193, 2014.

[11] Z. Nannan, Z. Q. Zhu, and L. Weiguo, "Rotor Eddy Current Loss Calculation and Thermal Analysis of Permanent Magnet Motor and Generator," *IEEE Trans. Magn.,* vol. 47, pp. 4199-4202, 2011.

[12] Y. Aoyama, K. Miyata, and K. Ohashi, "Simulations and experiments on eddy current in Nd-Fe-B magnet," *IEEE Trans. Magn.,* vol. 41, pp. 3790-3792, 2005.

[13] P. Sergeant and A. Van den Bossche, "Segmentation of Magnets to Reduce Losses in Permanent-Magnet Synchronous Machines," *IEEE Trans. Magn.,* vol. 44, pp. 4409-4412, 2008.

[14] K. Yamazaki, M. Shina, M. Miwa, and J. Hagiwara, "Investigation of Eddy Current Loss in Divided Nd–Fe–B Sintered Magnets for Synchronous Motors Due to Insulation Resistance and Frequency," *IEEE Trans. Magn.,* vol. 44, pp. 4269-4272, 2008.

[15] K. Yamazaki, M. Shina, Y. Kanou, M. Miwa, and J. Hagiwara, "Effect of Eddy Current Loss Reduction by Segmentation of Magnets in Synchronous Motors: Difference Between Interior and Surface Types," *IEEE Trans. Magn.,* vol. 45, pp. 4756-4759, 2009.

[16] K. Yamazaki, Y. Kanou, Y. Fukushima, S. Ohki, A. Nezu, T. Ikemi, *et al.*, "Reduction of Magnet Eddy-Current Loss in Interior Permanent-Magnet Motors With Concentrated Windings," *IEEE Trans. Ind. Appl.,* vol. 46, pp. 2434-2441, 2010.

[17] D. Liu, A. Jassal, H. Polinder, and J. A. Ferreira, "Validation of eddy current loss models for permanent magnet machines with fractional-slot concentrated windings," in *Proc. IEEE IEMDC*, 2013, pp. 678-685.

[18] K. Yamazaki, T. Fukuoka, K. Akatsu, N. Nakao, and A. Ruderman, "Investigation of Locked Rotor Test for Estimation of Magnet PWM Carrier Eddy Current Loss in Synchronous Machines," *IEEE Trans. Magn.,* vol. 48, pp. 3327-3330, 2012.

[19] L. Chen, J. Wang, and S. S. Nair, "An analytical method for predicting 3D eddy current loss in permanent magnet machines based on generalized image theory," *IEEE Trans. Magn.,* vol. PP, pp. 1-1, 2015.

[20] S. S. Nair, L. Chen, J. Wang, R. Chin, I.Manolas, and D.Svechkarenko, "Computationally efficient 3D analytical magnet loss prediction in SPM machines," *Electric Power Applications, IET,* vol. pp, pp. 1-25, 2016 (Early Access).

[21] S. S. Nair, J. Wang, L. Chen, R. Chin, I. Manolas, and D. Svechkarenko, "Computationally efficient 3D rotor eddy current loss prediction in permanent magnet machines," in *2016 XXII International Conference on Electrical Machines (ICEM)*, 2016, pp. 1426-1432.

[22] S. S. Nair, J. Wang, L. Chen, R. Chin, I. Manolas, and D. Svechkarenko, "Prediction of 3-D High-Frequency Eddy Current Loss in Rotor Magnets of SPM Machines," *IEEE Trans. Magn.,* vol. 52, pp. 1-10, 2016.

[23] P. Lazari, J. Wang, and C. Liang, "A Computationally Efficient Design Technique for Electric-Vehicle Traction Machines," *IEEE Trans. Ind. Appl.,* vol. 50, pp. 3203-3213, 2014.

[24] L. J. Wu, Z. Q. Zhu, D. Staton, M. Popescu, and D. Hawkins, "Analytical Model for Predicting Magnet Loss of Surface-Mounted Permanent Magnet Machines Accounting for Slotting Effect and Load," *IEEE Trans. Magn.,* vol. 48, pp. 107-117, 2012.

[25] B. Aslan, E. Semail, and J. Legranger, "General Analytical Model of Magnet Average Eddy-Current Volume Losses for Comparison of Multiphase PM Machines With Concentrated Winding," *IEEE Trans. Energy Convers.,* vol. 29, pp. 72-83, 2014.